Modal analysis of concentration information in a magnetic micromixer

F. Gökhan Ergin[1,*], Guntars Kitenbergs[2], Andrejs Cēbers[2]

1: Dantec Dynamics, Skovlunde, Denmark
2: University of Latvia, MMML lab, Riga, Latvia
*Corresponding author: gokhan.ergin@dantecdynamics.com

Keywords: Magnetic Micromixer, Magnetic microconvection, Concentration measurement, Proper Orthogonal Decomposition

ABSTRACT

Mixing is one of the most frequently used processes in microfluidic devices and Lab-on-a-Chip applications, therefore subtantial flow field investigation efforts are spent to achieve high performance micromixers. In this work, we revisit a magnetic micromixer experiment reported by Ergin et al. (2013) and Ergin et al. (2019), where velocity, concentration and interface investigations had been carried out. The magnetic micromixer exploits a phenomenon called magnetic microconvection, which appears on an interface of miscible magnetic and nonmagnetic fluids. Initial qualitative concentration measurements reported in Ergin et al. (2013) was improved by Ergin et al. (2019), both in terms of accuracy and resolution. The improvements in the experimental setup, improved microfluidic channel geometry, more accurate syringe pumps and inclusion of a concentration calibration step resulted in an accurate, time resolved and quantitative description of the concentration information for magnetic microconvection. In the current work we perform a modal analysis of the concentration field using Proper Orthogonal Decomposition (POD). The modal information provides crucial details about the mixing process at the interface for the magnetic microconvection phenomenon, giving a way to characterize and improve such mixers.

1. Introduction

Microfluidics technologies and lab-on-a-chip devices are gradually being introduced in the market, but mixing in diffusion limited laminar flows remains an important challenge. A lot of effort has been invested to investigate processes and systems that improve mixing. Use of magnetic materials is particularly attractive, as they can be actuated from distance. (Chen & Zhang (2017)). Here we revisit a magnetic micromixer experiment, which exploits a phenomenon called magnetic microconvection. (Ergin et al. (2013, 2019); Kitenbergs, Ērglis, et al. (2015)). Briefly, the magnetic micromixer works on the interface of miscible magnetic and nonmagnetic fluids in a thin layer. When the magnetic field is applied, the magnetic microconvection instability appears on the interface and a particular finger like pattern is formed. Compared to other mixers, a lot of work

has been done on explaining the phenomenon and formulating a theoretical model. (Kitenbergs, Tatulcenkovs, et al. (2015)). In addition, it has been investigated also in other geometries, such as in radial (Li et al. (2018)) and sessile droplets. (Lee et al. (2018)).

Quantitative characterization of mixing flows at an interface requires a detailed comparison and analysis of velocity, concentration and interface information. This requires the accurate measurement of each using techniques such as Particle image velocimetry (PIV) (Ergin et al. (2018)), light absorbtion and Phase boundary detection (PBD) (Ergin et al. (2020)) techniques, respectively. Initial velocity, concentration and interface measurements were reported in Ergin et al. (2013), where the velocity information was obtained using MicroPIV and Least Squares Matching (LSM). Proof-of-concept concentration measurements were made assuming a linear change in absorption with concentration. Finally, qualitative, preliminary interface front measurements were made using a series of image processing functions including the Prewitt edge detection filter. Later the experiment and analysis were improved on several points in Ergin et al. (2019), both in terms of accuracy and resolution. First improvement was about better control of the gravitational forces on the setup: During a magnetic microconvection investigation, it was noticed that even the tiny channel thickness is sufficient for gravity induced convection (Kitenbergs et al. (2018)), where denser magnetic fluid wants to slide below the less dense water. To eliminate the unwanted convection, we decided to position the sample vertically, placing denser magnetic fluid below the less dense water. In order to achieve this, the entire microscope and corresponding microPIV system was laid sideways on the table. Although this did not look pretty, it succeeded in diminishing the unwanted gravity effects (see Fig. 1).

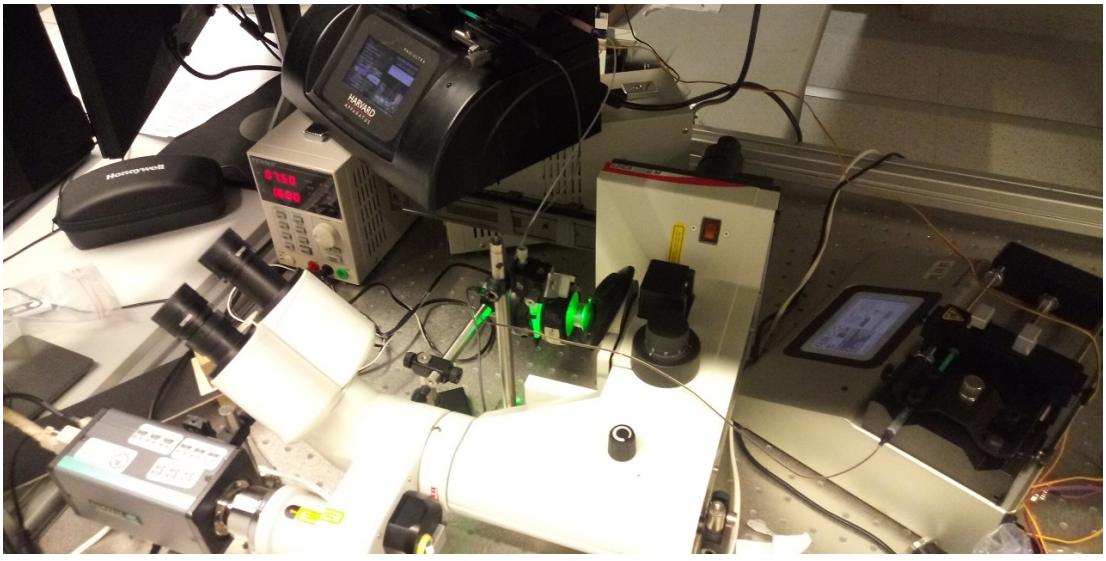

Figure 1. An image of the experimental setup, which is based on Dantec Dynamics MicroPIV system that is complemented by a magnetic coil and microfluidics system.

The second improvement in Ergin et al. (2019) was the inclusion of two syringe pumps: The magnetic and non-magnetic fluids were introduced and extracted by two syringe pumps, which are synchronized by an Arduino control. This allows to start and stop flow in a highly controlled

manner. The third improvement was the inclusion of a concentration calibration procedure (see Fig. 2), which produced a quantitative concentration information. The 90°-rotation of the experimental setup eliminated the magnetic fluid slip under water, which allowed to study microflows in a more true 2D environment. In addition, the advanced fluid control allows to form a flat interface. These improvements make the experiment much closer to theoretical model and simulations (Kitenbergs, Tatulcenkovs, et al. (2015)) and allow a better comparison between them. Alternatively the gravitational influence can be eliminated by using notably thinner channels (Kitenbergs & Cēbers (2020)) - this allows to use flat cells, but reduces the microconvection effect and our ability to study it.

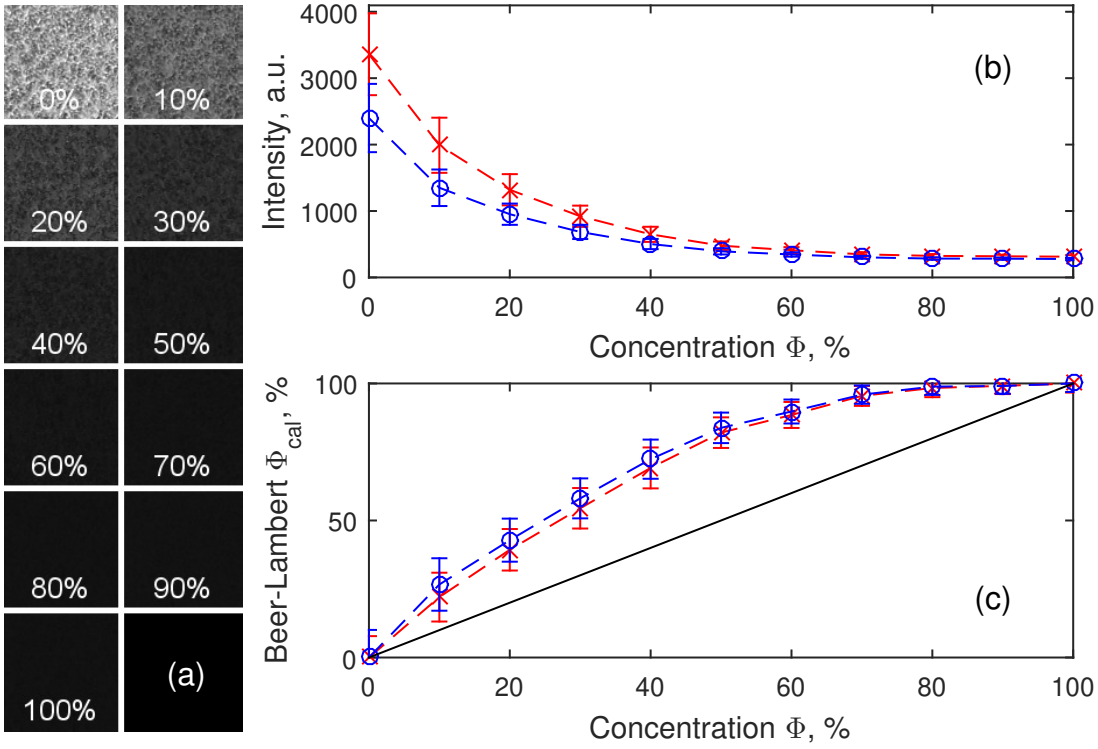

Figure 2. Magnetic fluid concentration calibration. (a) sample images for various magnetic fluid concentrations. (b) Average intensity dependence on magnetic fluid concentration for two different microstrobe pulse lengths, t_p. (c) Comparison between real magnetic fluid concentrations and values expected from Beer-Lambert law. In (b) and (c) Red crosses correspond to $t_p = 750$ μs, while blue circles to $t_p = 500$ μs. Black line in (c) indicates a linear change in absorption with concentrations, assumed in earlier publications.

2. Experiment Setup

Experiments were performed using an experimental setup based on a MicroPIV system manufactured by Dantec Dynamics. MicroPIV system consists of a HiPerformance inverted fluorescense microscope (based on Leica DMIL), double-frame PIV camera HiSense MkII, green LED Microstrobe pulsed illumination, 80N77 timer box and a computer equipped with DynamicStudio software v6.2. It is complemented by a custom magnetic coil that is powered by a power supply

(TENMA) and can create homogeneous magnetic fields ranging from 0 to 10 mT. To enable microflows, a microfluidics channel, tubing and microfluidic syringe pumps (Harvard Apparatus, KD Scientific) are used. The microfluidics channel is made in a simple but robust manner. We use a Parafilm®M spacer, in which channels are cut by a paper knife. Then this spacer is sandwiched between two microscope glass slides and heated on a hotplate until it makes a sealed channel. Syringe tips are glued in the drilled holes of the top glass slide and work as tubing connectors. For the magnetic fluid we used maghemite nanoparticle colloid (made in PHENIX lab, Paris, France) with a volume fraction $\Phi = 2.8\%$, nanoparticle average diameter $d = 7.0$ nm, saturation magnetization $M_{sat} = 8.4$ G and magnetic susceptibility $\chi_m = 0.016$, as determined by a vibrating sample magnetometer (Lake Shore 7404). The miscible nonmagnetic fluid was deionized water. In order to visualize the flow, we add $\Phi = 0.1\%$ plastic tracer particles with the average diameter $d = 1.0$ μm (Invitrogen). The microstrobe illumination is placed on the opposite side of the microfluidics cell, providing bright field microscopy conditions. Hence, tracer particles provide contrast, but no fluorescent signal.

The experiment procedure consists of the following steps: First, both fluids are introduced in chip with the same speed 50 μl/min, forming a sharp and moving interface. At the same time fluids are extracted from the outlet at a double speed 100 μl/min. Then the flows are stopped using synchronized control. Once interface stops, magnetic field is turned on. The process is recorded with the MicroPIV system, using 750 μs microstrobe double pulses at 6 Hz. The 0.7 x camera mount and the 10 x microscope objective produces a total system magnification 7 x. This produces a 1.238×0.943 mm^2 field of view. The recorded images are then subject to image pre-processing, concentration calculation using the calibration information and subsequent POD computation. The entire image pre-processing, calibration and modal analyses are performed using DynamicStudio software.

3. Concentration calibration

The acquired images are pre-processed following the same procedure as in Ergin et al. (2010). As compared to previous magnetic microconvection PIV measurements (Ergin et al. (2013); Ērglis et al. (2013)), the experiment quality and image quality was increased substantially. The interface is initially straight and the finger formation is clearly visible and symmetric around the initially straight interface. If the intensities of water and initial magnetic fluid are known at the beginning of the experiment before mixing, the concentration can be expressed as a function of image intensities. Whereas, Ergin et al. (2013) used a linear expression, Ergin et al. (2019) used a logarithmic expression based on a Beer-Lambert law. Ergin et al. (2019) also showed that the logarithmic expression alone is insufficient and an additional calibration step is needed:

$$\Phi_{cal}(x,y) = \frac{\log_{10} I(x,y) - \log_{10} I_{H_2O}}{\log_{10} I_{MF} - \log_{10} I_{H2O}}, \tag{1}$$

where $I(x, y)$ is the light intensity in point (x,y), I_{H_2O} is the average intensity of water and I_{MF} is the average intensity of original magnetic fluid. This logarithmic relation also includes 2 constants, which can be computed during calibration.

For calibration we prepare 11 samples with different concentrations of original magnetic fluid with tracer particles, by mixing it with water with tracer particles, so that we obtain magnetic fluid concentrations 0%, 10%, .. 100%. Each of the samples is imaged using the same system and settings as experimental images of the magnetic microconvection. Sample images (with 0.25×0.25 mm^2 region of interest) can be seen in Fig. 2 (a). One can easily see that the magnetic fluid concentrations above 50% are already quite dark. To measure this quantitatively, we find the average intensity and its error (standard deviation) for each image with a different concentration. We do this for 2 different Microstrobe pulse lengths. As a result, we find an intensity decrease with an increase of magnetic fluid concentration that should be expected (Fig. 2 (b)).

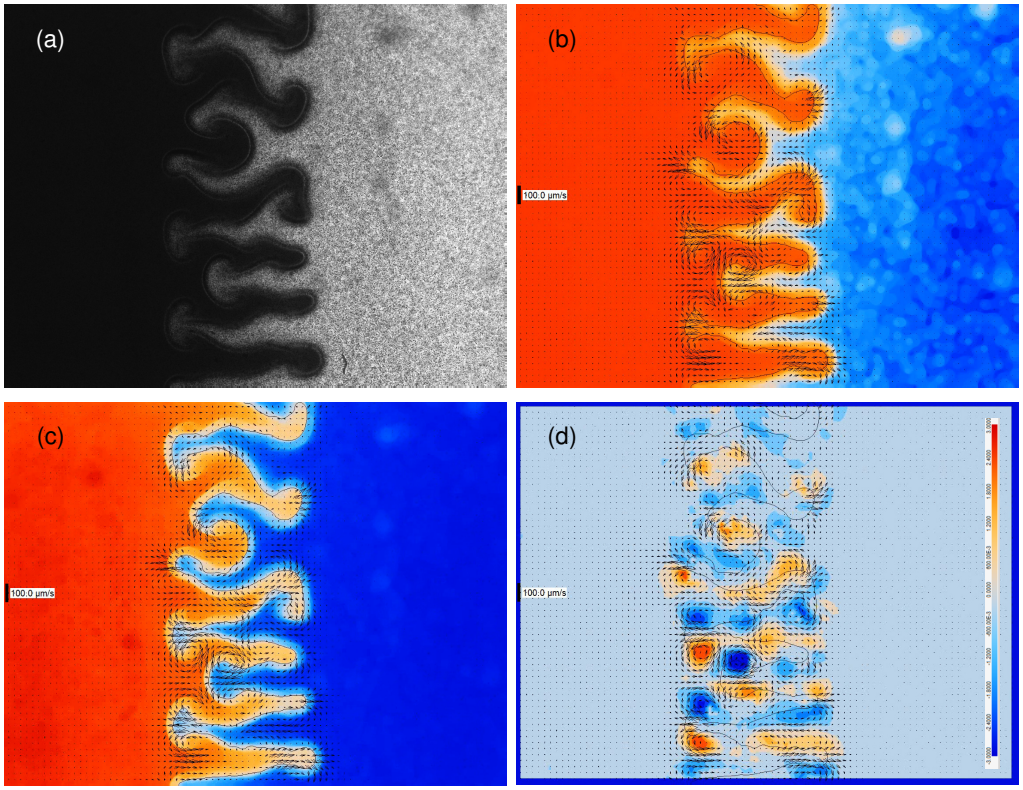

Figure 3. An example of image processing results. (a) Original snapshot of the magnetic microconvection. (b) Concentration plot assuming linear dependence. (c) Concentration plot using Beer-Lambert calibration (assuming logarithmic change). (d) Vorticity plot. All three (b), (c) and (d) show also phase boundary and flow field.

Fig 3 can be used to demonstrate why a concentration calibration must be performed during light absorption measurements. Fig 3 (a) shows the sample raw image of the experiment where magnetic fluid is on the left and non-magnetic fluid is on the right. Both phases are seeded with the same particles. Fig 3 (b) shows the concentration field assuming a linear change in concentration with transmitted light intensity as assumed in Ergin et al. (2013) (black line in Fig. 2 (c)). Fig 3 (c)

shows the concentration field assuming a logarithmic change in concentration with transmitted light intensity as assumed in Ergin et al. (2019) (blue and green lines in Fig. 2 (c)). Fig 3 (d) shows the vorticity map and the interface. When Fig 3 (b) and Fig 3 (c) are compared the necessity of performing a concentration calibration is obvious. Without performing calibration Fig 3 (b) the concentration gradient does not coincide with the mixing interface and spills over towards the non-magnetic fluid, which is not physical. However with calibration, Fig 3 (c), the concentration distribution is corrected; the concentration gradient coincides with the mixing interface, is much more symmetric on both sides of the interface and moves together with the interface throughout the experiment. Also vorticity dynamics displays the few strong vortices in the beginning, many less strong vortices in the middle and a few vortices further away from the phase boundary, indicating the decay of the convective motion. Both findings qualitatively agree very well with numerical simulations (Kitenbergs, Tatulcenkovs, et al. (2015)).

4. Proper Orthogonal Decomposition

A Proper Orthogonal Decomposition (POD) analysis was performed on a similar magnetic microconvection experiment by Ergin et al. (2014) on time-resolved velocity data. Here we perform POD on the scalar concentration data. Briefly, POD is a powerful method for system identification aiming at obtaining low-dimensional approximate descriptions for multi-dimensional systems. POD provides a basis for the modal decomposition of a system of functions, as in the case of data acquired through experiments. It provides an efficient way of capturing dominant components of a multi-dimensional system and representing it with a desired precision by using a relevant set of modes, thus reducing the order of the system. POD is closely related to Principal Component Analysis (PCA) from linear algebra. In its original form, it derives only spatial modes which are mutually orthogonal. Temporally, each mode provides varying contributions to the individual datasets (snapshots) and it turns out that these temporal 'modes' are also mutually orthogonal. This was formally described in 1991 by Aubry et al. (1991), who proposed the name 'Bi-Orthogonal Decomposition' to emphasize the orthogonality of both spatial and temporal modes. They also proposed the name 'Topos' to describe spatial modes and 'Chronos' to describe temporal modes. In this paper, we use the name 'Proper Orthogonal Decomposition' since it is by now an established and accepted technique, but we adopt the names 'Topos' and 'Chronos' to describe spatial and temporal modes, respectively. Each instantaneous concentration measurement is considered as a snapshot of the concentration field. If an ensemble of concentration maps acquired in the same position and under identical experimental conditions is available, POD subtracts the temporal mean and performs a full spatio-temporal decomposition of the fluctuating part of the concentration such that the instantaneous concentration field $C(x, y, t)$ can be reconstructed from a series of K modes:

$$C(x, y, t) = \sum_{k=0}^{K-1} \sigma_k \Phi_k(x, y) \Psi_k(t) \tag{2}$$

where σ_k is the global amplitude of the kth mode, Φ_k is the kth 'Topos' (spatial mode), and Ψ_k is the kth 'Chronos' (temporal mode). The amplitude, Topos and Chronos of mode 0 ($k = 0$) describe the mean concentration field, and the remaining Topos and Chronos are orthonormal:

$$\langle \Phi_i, \Phi_j \rangle = \langle \Psi_i, \Psi_j \rangle = \delta_{ij} \tag{3}$$

The modes are sorted by the amplitude (concentration deviation squared) such that the first mode is the one contributing to the largest fraction of the total energy and the subsequent modes contribute to smaller and smaller fractions thereof. The first modes will typically be associated with large-scale flow structures, and the last modes will typically describe only the measurement noise. The modal decomposition methods are described in a review by Uruba (2012).

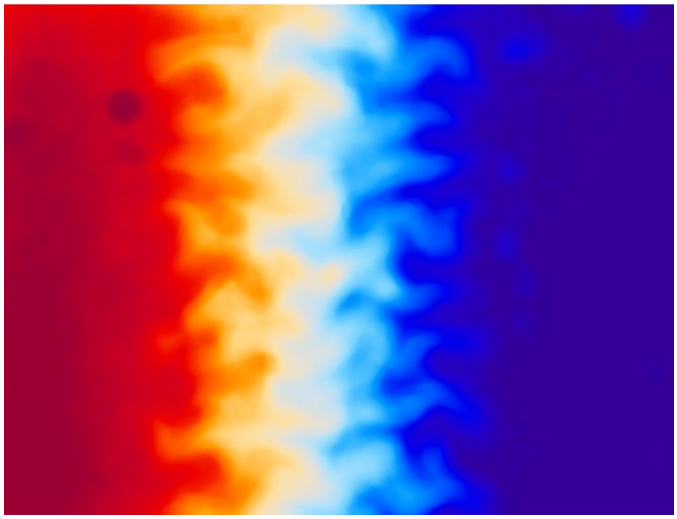

Figure 4. POD Mode 0: the time-average concentration field.

5. Results

The 0^{th} Topos is the time-average of the POD input, in this case the mean concentration field (Fig. 4). The subsequent 4 Topos are shown in Fig. 5, and their temporal counterparts (Chronos) are shown in Fig. 6. The computed POD modes are ranked by their kinetic energy amplitude such that the first mode is the one contributing to the largest fraction of the total energy and the subsequent modes contribute to smaller and smaller fractions thereof. As a result of this, the first modes will typically be associated with largescale flow structures, and the subsequent modes will typically have smaller and smaller flow structures (Fig. 5) with increasing frequencies (Fig. 6). It is interesting to note that nth Chronos always have $n - 1$ peaks.

The first few Topos and Chronos appear to characterize the microconvective mixing behavior quite well. For example, Topos 1 (Fig. 5 (a)) indicates 7 pairs of red and blue protrusions at the initial interface area, which agree with the 7 finger-like structures of convective flow, visible in Fig. 3 (c). At this stage the fingers have not really begun sliding within eachother, but they are about to.

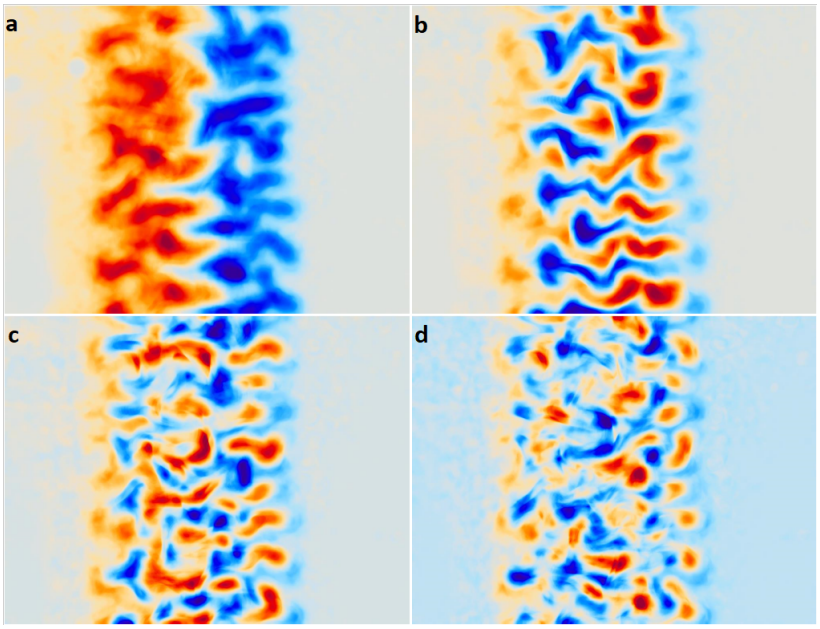

Figure 5. Topos 1, 2, 3, and 4: The 1st 4 spatial POD modes of the concentration field.

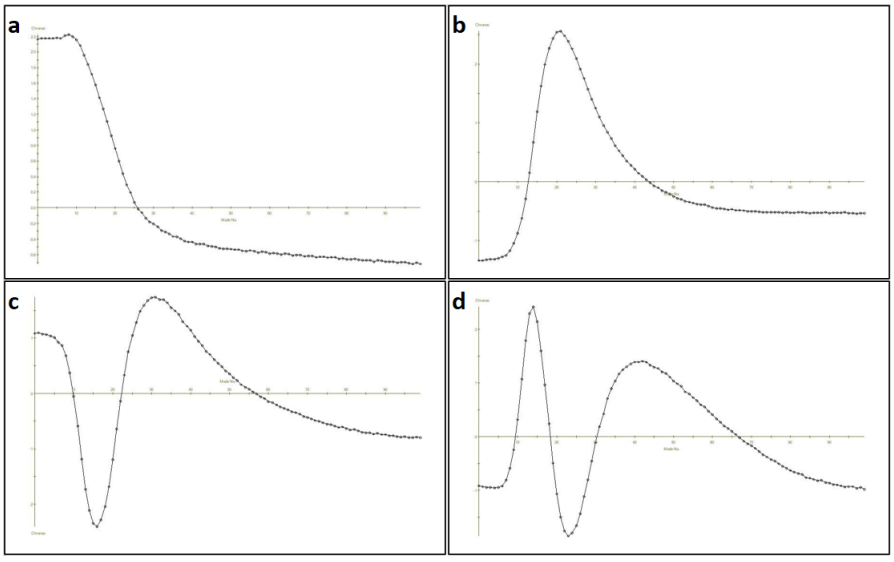

Figure 6. Chronos 1, 2, 3, and 4: The 1st 4 temporal POD modes of the concentration field.

This is initial fingering pattern and develops at the beginning of the mixing, which agrees with the dynamics of Chronos 1 (Fig. 6 (a)), where the amplitude remains high until time frame ≈ 13. Topos 2 (Fig. 5 (b)) not only shows clearly the 7 pairs of fingers which have slid into each other, but it also shows the mushroom-like finger tips that lead to splitting of instability driven fingers (see them also in Fig. 3 (c)). This is a clear change of mixing dynamics and also here Chronos 2 (Fig. 6 (b)) reflects it well, as the amplitude increases and peaks around time frame ≈ 20. This coincides with the best pronounced mushroom-like tips and the start of finger splitting.

From the complex convective motion, we can note two characteristics that should be the most important for mixing. First is the lateral movement of fluids across the interface, which is done by

initial fingering pattern and, as discussed above, is characterized by Topos 1 and Chronos 1. We know from finger velocity measurements in Kitenbergs, Tatulcenkovs, et al. (2015) that the finger formation speed depends on the square of magnetic field applied. Therefore, we can propose a hypothesis that larger magnetic field should result in a larger amplitude in Topos 1 as well as a shorter dynamics of Chronos 1. Second is the finger splitting, which enhances mixing and splits the otherwise finger-like pattern. From previous studies it is clear that a certain magnetic field is needed for this and here oberving Topos 2 and Chronos 2 should show a change in behavior across this threshold. However, more research is needed to prove these hypotheses.

Further modes of Topos and Chronos seem to describe additional details of the complex convective process and its dynamics and could help to better describe secondary fingering (Wen et al. (2007)) and other phenomena in complex mixers. It would also be interesting to see if similarities in POD analysis can be seen with other recent propositions of magnetic micromixers (Coutinho & Miranda (2020); Krakov et al. (2021)) both experimentally and numerically.

6. Conclusions

We have shown that POD analysis can be successfully applied to concentration dynamics of a micromixer and it allows to retrieve characteristics of interest both to study the physics of microconvective flows and for the possibility to improve the micromixer. Here the first two modes of Chronos and Topos seem to well describe the initial instability formation and growth, as well as transition to a more complex flow of the magnetic microconvection. However, more research needs to be done to generalize the applicability of POD analysis and the conditions to do that.

Acknowledgements

We thank D. Talbot (PHENIX lab, Sorbonne University in Paris, France) for the magnetic fluid and I. Drikis for an Android based synchronization solution for microfluidics pumps. G. Kitenbergs' research has been funded by a PostDocLatvia project Nr.1.1.1.2/VIAA/1/16/197.

References

Aubry, N., Guyonnet, R., & Lima, R. (1991). Spatiotemporal analysis of complex signals: Theory and applications. *Journal of Statistical Physics*, *65*(3), 683-739. doi:

Chen, X., & Zhang, L. (2017, Oct 01). A review on micromixers actuated with magnetic nanomaterials. *Microchimica Acta*, *184*(10), 3639–3649. Retrieved from `https://doi.org/10.1007/s00604-017-2462-2` doi:

Coutinho, I. M., & Miranda, J. A. (2020). Peak instability in an elastic interface ferrofluid. *Physics of Fluids*, *32*(5).

Ergin, F. G., Kitenbergs, G., & Cēbers, A. (2019). Revisiting velocity, concentration and interface measurements in a magnetic micromixer. In *13th international symposium on particle image velocimetry - ispiv19, munich, germany, july 22-24.*

Ergin, F. G., Olofsson, J., Petersson, P., & Gade-Nielsen, N. F. (2020). A hybrid phase boundary detection technique for two-phase-flow piv measurements. *Flow Measurement and Instrumentation*, *74*, 101776. Retrieved from https://www.sciencedirect.com/science/article/pii/S0955598620301229 doi:

Ergin, F. G., Watz, B., & Gade-Nielsen, N. (2018, Sep). A review of planar piv systems and image processing tools for lab-on-chip microfluidics. *Sensors*, *18*(9), 3090. Retrieved from http://dx.doi.org/10.3390/s18093090 doi:

Ergin, F. G., Watz, B. B., Ērglis, K., & Cēbers, A. (2010). Poor-Contrast Particle Image Processing in Microscale Mixing. In *Asme 2010 10th biennial conference on engineering systems design and analysis - istambul, turkey, jul 12-14.*

Ergin, F. G., Watz, B. B., Ērglis, K., & Cēbers, A. (2013). Planar velocity and concentration measurements in a magnetic micromixer with interface front detection. In *10th international symposium on particle image velocimetry - piv13, delft, the netherlands, july 1-3.*

Ergin, F. G., Watz, B. B., Ērglis, K., & Cēbers, A. (2014). Modal analysis of magnetic micro-convection. *Magnetohydrodynamics*, *50*(4), 339 - 352. Retrieved from http://mhd.sal.lv/contents/2014/4/MG.50.4.1.R.html doi:

Ērglis, K., Tatulcenkov, A., Kitenbergs, G., Petrichenko, O., Ergin, F. G., Watz, B. B., & Cēbers, A. (2013). Magnetic field driven micro-convection in the hele-shaw cell. *Journal of Fluid Mechanics*, *714*, 612–633. doi:

Kitenbergs, G., & Cēbers, A. (2020). Rivalry of diffusion, external field and gravity in micro-convection of magnetic colloids. *Journal of Magnetism and Magnetic Materials*, *498*, 166247. Retrieved from https://www.sciencedirect.com/science/article/pii/S0304885319327714 doi:

Kitenbergs, G., Ērglis, K., Perzynski, R., & Cēbers, A. (2015). Magnetic particle mixing with magnetic micro-convection for microfluidics. *Journal of Magnetism and Magnetic Materials*, *380*, 227 - 230. Retrieved from http://www.sciencedirect.com/science/article/pii/S0304885314009330 doi:

Kitenbergs, G., Tatulcenkovs, A., Ērglis, K., Petrichenko, O., Perzynski, R., & Cēbers, A. (2015). Magnetic field driven micro-convection in the hele-shaw cell: the brinkman model and its comparison with experiment. *Journal of Fluid Mechanics*, *774*, 170–191. doi:

Kitenbergs, G., Tatulcenkovs, A., Pukina, L., & Cēbers, A. (2018). Gravity effects on mixing with magnetic micro-convection in microfluidics. *Eur. Phys. J. E*, *41*(11), 138. Retrieved from https://doi.org/10.1140/epje/i2018-11749-9 doi:

Krakov, M. S., Zakinyan, A. R., & Zakinyan, A. A. (2021). Instability of the miscible magnetic/non-magnetic fluid interface. *Journal of Fluid Mechanics*, *913*. Retrieved from www.scopus.com (Cited By :1)

Lee, J. G., Porter, V., Shelton, W. A., & Bharti, B. (2018). Magnetic field-driven convection for directed surface patterning of colloids. *Langmuir*, *34*(50), 15416-15424. doi:

Li, H., Kao, C.-Y., & Wen, C.-Y. (2018). Labyrinthine and secondary wave instabilities of a miscible magnetic fluid drop in a hele-shaw cell. *Journal of Fluid Mechanics*, *836*, 374–396. doi:

Uruba, V. (2012). Decomposition methods in turbulence research. *EPJ Web of Conferences*, *25*, 01095. Retrieved from https://doi.org/10.1051/epjconf/20122501095 doi:

Wen, C.-Y., Chen, C.-Y., & Kuan, D.-C. (2007). Experimental studies of labyrinthine instabilities of miscible ferrofluids in a hele-shaw cell. *Physics of Fluids*, *19*(8), 084101. doi: